This is the peer reviewed version of the following article: F. Fanelli, R. d'Agostino, F. Fracassi, Effect of gas impurities on the operation of dielectric barrier discharges fed with He, Ar and Ar-C_3F_6, Plasma Processes and Polymers 2011, 8, 557–567, which has been published in final form at https://doi.org/10.1002/ppap.201000179. This article may be used for non-commercial purposes in accordance with Wiley Terms and Conditions for Use of Self-Archived Versions. This article may not be enhanced, enriched or otherwise transformed into a derivative work, without express permission from Wiley or by statutory rights under applicable legislation. Copyright notices must not be removed, obscured or modified. The article must be linked to Wiley's version of record on Wiley Online Library and any embedding, framing or otherwise making available the article or pages thereof by third parties from platforms, services and websites other than Wiley Online Library must be prohibited.

Article Type: Full Paper

Effect of Gas Impurities on the Operation of Dielectric Barrier Discharges fed with He, Ar and Ar-C_3F_6

Fiorenza Fanelli,* Riccardo d'Agostino, Francesco Fracassi

F. Fanelli, R. d'Agostino, F. Fracassi
Dipartimento di Chimica, Università degli Studi di Bari Aldo Moro–IMIP CNR, via Orabona 4, 70126 Bari, Italy
Fax: +39 0805443405; E-mail: fiorenzafanelli@chimica.uniba.it

---

Summary

The influence of N_2, O_2, air and water vapor feed gas impurities on the operation of an atmospheric pressure parallel plate DBD fed with helium and argon was investigated. The addition of increasing amounts of these impurities, under fixed excitation frequency and applied voltage, is responsible above certain thresholds of two distinct phenomena, namely the transition from a homogeneous to a filamentary appearance of the discharge and the contraction of the discharge volume. Among the different contaminants N_2 shows the highest threshold limit values, O_2 and H_2O the lowest ones, while air generally exhibits an intermediate behavior.

The effect of feed gas impurities was also studied on the PE-CVD of fluoropolymers from Ar-C_3F_6 fed filamentary DBDs. Contaminants addition results in a decrease of the input power and of the deposition rate as well as in a change of the film morphology, however it does not influence significantly the chemical composition of the fluoropolymer film, the monomer depletion and the distribution of by-products in the exhaust gas.

Introduction

The dielectric barrier discharge (DBD) is a very popular experimental methodology to establish non-equilibrium plasma conditions at atmospheric pressure.[1-5] Over the last few years it has attracted growing interest in surface processing of materials; the intense research activity in this field has been motivated by the potential advantages of the atmospheric pressure operation; the absence of vacuum equipments is, in fact, expected to result in cost reduction of processes and reactors, in the easier utilization and maintenance of apparatuses, as well as in the simple integration into on-line production.

The confident utilization of DBDs in surface treatment of materials strictly requires the knowledge of the most important aspects of their operational features which highly differentiate this approach from the well-established low pressure plasma technology.

The most important peculiarity of DBDs, which often complicate their employment in surface processing of materials, is the existence of completely different discharge regimes;[1-15] two major discharge modes are reported in the literature: the filamentary regime and the homogeneous or diffuse regime.

In most cases DBDs operate in the filamentary regime (i.e. filamentary dielectric barrier discharges, FDBD) characterized by an intrinsically inhomogeneous structure consisting of many microdischarges (MDs) randomly distributed in time and space in the discharge gap over the dielectric surface.[1-6] A microdischarge is a short living (< 100 ns time duration) constricted (< 200 μm diameter) discharge channel. According to the recent nomenclature on FDBDs proposed by Fridman et al.,[4, 5] a microdischarge is defined as the group of the following local processes: (i) formation of a streamer from the amplification of a primary avalanche, (ii) streamer

propagation, (iii) formation of a discharge channel which bridges the gas gap, (iv) discharge channel extinction due to the collapse of the local electric field induced by the dielectric layer. A filament is a group of microdischarges which form repeatedly at the same spot and can be detected with the naked eye. The MDs statistical distribution should confer to the FDBD an overall uniform appearance, however at the usual operation frequencies (around 20 kHz) MDs repeatedly form at the same locations as the polarity of the applied voltage changes, and hence can be macroscopically observed as bright spatially localized filaments.[4, 5]

Under particular experimental conditions, homogeneous microdischarge-free regimes can be obtained. Two forms of homogeneous discharge can be generally observed: the glow-like discharges and the Townsend-like discharges.[8-11] Homogeneous DBDs fed by noble gases (e.g. helium[8-15]) are qualified as glow-like discharges (atmospheric pressure glow discharges, APGD, or glow dielectric barrier discharges, GDBD), characterized by the formation in the region near to the instantaneous cathode of a positive space charge which produces a strong electric field variation known as cathode voltage fall. Typical APGD current densities range between 10 and 100 $mA \cdot cm^{-2}$, while the maximum electron density is about 10^{10} - 10^{11} cm^{-3}.[10] The low-current homogeneous discharges obtained in molecular gases such as N_2[9-11, 17] are referred to as Townsend-like discharges (atmospheric pressure Townsend discharges, APTD, or Townsend dielectric barrier discharges, TDBD). These are characterized by a relatively small space charge which does not affect the electric field. In this case, in fact, the ionization level is not high enough to induce the formation of a cathode fall and hence the electric field remains quasi-uniform over the discharge gap. In an APTD the current density and the maximum electron density are in the range ~ 0.1 – 10 $mA \cdot cm^{-2}$ and ~ 10^7 – 10^8 cm^{-3}, respectively.[9-10] It is worth mentioning the existence of some particularities or exceptions from the above described homogeneous regimes, e.g. the pseudo-glow regime observed in noble gases.[14, 27, 30, 31]

Several diagnostic techniques, such as the discharge current signal acquisition,[7-10] the total light emission measurement[18] and the high-speed imaging,[7-10, 19-21] have been employed to assess and monitor the DBD regime. Despite the great deal of work produced, the multiplicity of electrode configurations, power supplies, gas mixtures and experimental conditions employed, an unanimous understanding and control of the homogeneous regimes, and of the transition between homogeneous and filamentary regimes, has not been achieved so far.[10] Several studies demonstrated, in fact, that the operational window and stability of homogeneous DBDs is strictly related to both the experimental conditions and the mechanical and electrical characteristics of the apparatuses, such as the feed mixture (i.e. main gas, nature and concentration of feed gas additives), the electrode configuration, the nature and permittivity of the dielectric material, the applied voltage, the excitation frequency, the power supply and the presence of additional elements in the external electrical circuit for impedance matching[22, 23] or electronic stabilization.[24-26]

The feed gas composition plays a decisive role in determining the existence domain and characteristics of the different DBD regimes. It seems, in fact, relatively easy to obtain homogeneous regimes in He and N_2, while contrasting results are reported for other gases such as Ar and air. Some authors reported that in pure argon a homogeneous regime can not be obtained unless low concentration of acetone[28] or ammonia[9] are added (the two additives allow to obtain a so-called Penning mixture which favours the glow DBD generation[9]), while other authors obtained homogeneous regimes in several pure gases (e.g. argon, air, oxygen, carbon dioxide, etc.) and in various feed gas mixtures.[13, 20-22, 28, 29]

The studies devoted to the investigation of the different discharge regimes and to the transition between them showed that the homogeneous discharges (e.g. He glow and N_2 Townsend DBDs) are extremely susceptible to feed gas additives (often referred to as “impurities”) which above

certain concentration levels may readily cause the transition from the homogeneous regime to the filamentary regime.[18, 27, 32, 33] For instance, Massines et al.[7] reported that 400 ppm of O_2 in N_2 can completely change the DBD mode from homogeneous to filamentary; Brandenburg et al.[27] showed that an air content higher than 800 ppm in He is responsible for both the homogeneous-to-filamentary transition and the increase of the voltage required to sustain the discharge.

The influence of feed gas additives on DBD operation was accurately evaluated, for instance, in the optimization of PE-CVD processes which require the addition of at least one compound (i.e. the film precursor) to the main gas. In the case of fluoropolymers deposition in helium-fluorocarbon fed DBDs we showed that the typical features of a glow DBD can be obtained at fluorocarbon concentrations lower than 0.01% and 0.025% for hexafluoropropene (C_3F_6) and octafluoropropane (C_3F_8), respectively.[33] However Aldea et al.,[24-26, 34] by using suitable electronic stabilization of the fast current variations to prevent glow-to-arc transition, dynamic matching and particular discharge assembly, demonstrated that the glow regime can be successfully achieved for a wide range of plasma parameters and for concentrations of additives up to 50% of feed.[24-26, 34] These results indicate that it is possible to enlarge the homogeneous discharge operational window and to obtain the homogeneous regime under experimental conditions very close to the practical applications and in cost-efficient He-free feed mixtures. Recent publications from Starostin et al.[19-21, 35] demonstrated, for instance, that it is possible to obtain uniform and high quality large area deposition of SiO_2-like layers with homogeneous DBDs fed by Ar-N_2-O_2-HMDSO [19, 20, 35] or air-Ar-HMDSO.[21] The formation and temporal evolution of the homogeneous discharge in these PE-CVD processes was studied by fast discharge imaging and electrical diagnostics.

In surface processing of materials, some efforts have been recently directed to evaluate if atmospheric pressure DBDs can be competitive with the low pressure plasma technology for some specific processes, such as polymer treatment and thin films deposition, which require also feed gases different from air. In this case, the possible presence of air and water vapor during the atmospheric pressure DBD processes should be seriously considered, in particular if vacuum pumps are absent and non-airtight apparatuses or even open air systems are employed. In fact, the presence of these impurities, besides influencing the discharge regime and operation, could have a serious detrimental effect on the overall performance of the plasma process. A possible case study is the atmospheric pressure PE-CVD of fluorocarbon thin films, in which air and water vapor contaminations could induce changes of the polymer composition, oxygen and nitrogen uptake, as well as variations of the deposition rate. On the other hand, the knowledge of the highest level of contamination compatible with acceptable performances could allow to reduce the cost of processes and reactors.

Hexafluoropropene is one of the most utilized fluorocarbon precursors in thin film deposition since it is characterized by a relatively low F/C ratio due to the presence of a carbon-carbon double bond. This accounts for the high polymerization rates both in low pressure[36-40] and atmospheric pressure plasmas.[33, 41-49] Low pressure C_3F_6-containing plasmas result in deposition rates as high as 350 $nm \cdot min^{-1}$[36, 37] and in coatings characterized by a maximum F/C ratio of 1.5.[36-40] Chen et al.[36] investigated the influence of O_2 and N_2 feed addition on the low pressure plasma polymerization of C_3F_6. Nitrogen and oxygen were incorporated in the deposit at atomic concentrations as high as 5% and 9%, respectively; the increase of the additives in the feed resulted in a decrease of the deposition rate which was steeper in the case of O_2 also for the chemical etching of the growing polymer. The F/C ratio of the coating decreased under O_2 addition, while a slight increase was observed with N_2.

Promising results on the fluoropolymers deposition from C_3F_6-containing DBDs were reported by several authors.[33, 41-49] In particular in He-C_3F_6 glow DBDs[33, 48] fluorocarbon films with F/C ratio of 1.5 were obtained with a deposition rate up to 34 $nm \cdot min^{-1}$.

In this paper we report a systematic study on the influence of feed gas contaminants on DBDs operation. Known concentrations of N_2, O_2, air and H_2O, were added to He and Ar fed DBDs in order to assess the discharge regime and overall stability; then the deposition of fluoropolymers from Ar-C_3F_6 FDBDs was evaluated as a function of the feed impurity level to determine the maximum extent of air and water vapor permissible without affecting the PE-CVD efficiency in terms of F/C ratio and deposition rate. The comparison between the characteristics of the deposited fluoropolymers and the exhaust composition determined by GC-MS (gaschormatography-mass spectrometry) allowed us to hypothesize some plasma reactive species and some features of the deposition mechanism.

Experimental

The experimental apparatus (**Figure 1**) consists of a parallel plate electrode system contained in an airtight Plexiglas box; each electrode of about 290 cm^2 area (21.0 cm long and 13.6 cm broad) is covered by one or two plates of dielectric material such as alumina (Coorstek, 96% purity, 0.635 mm thickness) and quartz (1.0 mm thickness), while the gas gap is varied between 1 and 5 mm.

The plasma is generated by applying an AC high voltage (up to 5.7 kV_{p-p}) in the frequency range between 5 and 20 kHz by means of a power supply composed of a variable frequency generator

(GW Instec GFG-8216A), an audio-amplifier (Outline PA4006, 3000 W) and a high voltage (HV) transformer (Montoux, 3000 VA, $90V_{rms}/3kV_{rms}$). The voltage applied to the electrodes (V) is measured by means of a high voltage probe (Tektronix P6015A, 75 MHz bandwidth, 1000 attenuation factor), while the current (I) flowing through the electrical circuit and the charge (Q) are evaluated by a voltage probe (Tektronix P2200, 6 MHz bandwidth/1 attenuation factor, 200 MHz bandwidth, 10 attenuation factor) measuring the drop across a 50 Ω resistor and a 100 nF capacitor connected in series with the ground electrode, respectively. The signals are visualized on a digital oscilloscope (Tektronix TDS2014, 100 MHz bandwidth, 2 GS/s sample rate) and transmitted to a PC by a communication module (TDS-CMA Tektronix) for real-time acquisitions of the electrical signals registered by the probes. The electrical signals employed for the definition of the discharge regime are acquired in single shot mode at the highest sample rate of the oscilloscope. The average power dissipated by the discharge is calculated as the integral over one cycle of the product of the applied voltage and the current (electrical signals acquired in average mode over 128 samples) divided by the period (power measurement error of 5%). In some cases the power was determined with the Manley method, and in particular the voltage-charge (V-Q) Lissajous figure; the results obtained with the two methods are in good agreement.

MKS electronic mass flow controllers (MFC) and an MKS 122 baratron allow to set flow rates and monitor the pressure, respectively. In order to avoid overpressure, the Plexiglas enclosure is slightly pumped with a rotary pump (Pfeiffer). Feed gas is introduced in the interelectrodic zone through a slit and pumped through a second slit positioned on the opposite side, therefore a longitudinal gas injection is realized. Gas flow by-pass is minimized by using two quartz spacers which laterally confine the interelectrode gap.

In this work, He (Air Liquide Helium alphagaz 1) or Argon (Air Liquide Argon alphagaz 1) were used as main gases at a flow rate of 6 slm and 4 slm, respectively. N_2 (Air Liquide, nitrogen 1),

O_2 (Air Liquide, oxygen 1), air (Air Liquide, 80% N_2 – 20 % O_2) and water vapor, were added as additives to the feed at a volume concentration as high as 2%. Water vapor was introduced into the reactor by a He or Ar stream bubbling through a water reservoir kept at 0°C. The effective amount of H_2O admitted into the reactor was evaluated by reservoir weight variation per unit time and, assuming an ideal gas behavior, it was converted to flow rate expressed in sccm.

Deposition processes were preformed with 4 slm Ar flow rate (ϕ_{Ar}) and 0.2% C_3F_6, while the contaminant concentration in the feed was increased up to 0.4%, 0.05%, 0.2% and 0.1% for nitrogen, oxygen, air and water vapor, respectively. Before each experiment the Plexiglas chamber was flushed with a high flow rate of main gas (6 slm) for 40 min.

Table 1 summarizes the experimental parameters employed in this work.

Photographs showing the side-view of the discharge gap were taken using a digital camera (Olympus).

The chemical composition of the deposited films was investigated by Fourier transform infrared spectroscopy (FT-IR) and X-ray Photoelectron Spectroscopy (XPS). A commercial Bruker Equinox 55 FT-IR interferometer was used to collect infrared absorption spectra (4 cm^{-1} resolution) of the deposited films; in order to minimize the effects of carbon dioxide and water vapor, the optical path inside the sample compartment was purged with nitrogen during each measurement. XPS analyses were performed using a Theta probe spectrometer (Thermo Electron Corporation) equipped with a monochromatic Al K_α X-ray source (1486.6 eV) operated at a spot size of 400 μm (corresponding to a power of 100 W). Survey (0-1100 eV) and high resolution spectra (C1s, F1s, O1s, N1s) were recorded at a pass energy of 150 and 50 eV, respectively. Spectra were acquired with a take-off angle (TOA) of 37° with respect to the sample surface. The C1s signal for the CF_2 component (292.5 eV) was used as internal standard for the correction

of the charging of the samples.[50] The best fitting of the C1s spectra was performed using Advantage Data Spectrum Processing software (Thermo Electron Corporation).

Surface wettability was evaluated by dynamic water contact angle (WCA) measurements, using a Ramé-Hart manual goniometer (model A-100). Advancing and receding contact angles (AWCA and RWCA) were measured according to the sessile drop method on both sides of five drops of double distilled water for each sample and the average value was calculated with a maximum uncertainty of ±3°.

Film thickness was evaluated on substrates partially masked during the deposition using an Alpha-Step® 500 KLA Tencor Surface profilometer. Scanning electron microscopy (SEM) analyses were carried out by a digital microscope EVO 40XVP (Zeiss) to probe the coatings topography; before analysis the specimens were sputter-coated with a 60 nm thick gold thin film.

In order to compare the results obtained under different experimental conditions the coatings characterization was carried out on films deposited in the middle of the interelectrode region, that is in the region at 8–13 cm from the gas entrance inside the discharge area. In order to evaluate the homogeneity of the deposition over the entire electrode surface, under some experimental conditions the coatings characterization was performed on film deposited in the regions at 1–6 cm, 8–13 cm and 15–20 cm from the gas entrance inside the discharge area (electrode length of 21 cm).

Optical emission spectroscopy (OES) was performed by collecting the UV-Vis spectra (200–900 nm) using an optical multichannel analyser (OMA), equipped with a ACTONSP-300i monochromator (0.300 m focal length, 1200 grooves/mm grating) and a CCD detector (SpectruMMTM 100B, Princeton Instruments). To exclude the interference of second order signals, in the wavelength range of 450–850 nm the spectra were registered using a long pass filter (cutoff wavelength of 450 nm).

A stainless steel liquid nitrogen trap, located between the reactor and the rotary pump, allowed to sample the stable species contained in the exhaust gas (Figure 1). Sampling was performed for two hours, then the trap was isolated from the system, the condensate was dissolved in hexane (Fluka, purity ≥ 99.0 %) and analysed by means of gas chromatography (GC) with mass spectrometric (MS) detection. The GC apparatus (GC 8000^{Top} Thermoquest Corporation) was equipped with an Alltech AT^{TM}-1ms capillary column (polydimethylsiloxane 0.25 μm thick stationary phase, length of 30 m, internal diameter of 0.25 mm). The analyses were performed with 2 sccm of He as carrier gas, at 200°C injector temperature and column temperature programmed from 30 to 200°C (2 min at 30 °C, linear heating rate of 10°C·min^{-1}, 5 min at 200°C). The separated products were analysed with a quadrupole mass spectrometer (Voyager, Finnigan, Thermoquest Corporation). Mass spectra at 70 eV were recorded in full scan mode in the m/z range 18 – 700. The products were identified by means of available libraries.[51] The extent of reacted C_3F_6, namely the C_3F_6 depletion percentage, was evaluated according to equation (1):

$$C_3F_{6\,depletion}(\%) = \frac{C_3F_{6\,off}(sccm) - C_3F_{6\,on}(sccm)}{C_3F_{6\,off}(sccm)} \cdot 100 \qquad (1)$$

where $C_3F_{6\,off}$ and $C_3F_{6\,on}$ are the precursor flow rates detected in the exhaust with discharge off and discharge on conditions, respectively. The maximum experimentally estimated uncertainty of the C_3F_6 depletion percentage is ±3%.

Results and Discussion

Helium and argon fed dielectric barrier discharges

In the first part of this work, devoted to investigate the operation of helium and argon fed DBDs with contaminant addition, the discharge regime was assessed by electrical measurements, namely real time acquisitions of the voltage and current signals, as well as by naked-eye evaluations of the discharge.

A homogeneous discharge is characterized by only one current peak per half-cycle of the applied voltage (a noticeable exception is represented by the multipeak signal of a pseudoglow discharge[14, 27, 30, 31]). All positive (or negative) peaks exhibit almost the same shape, amplitude and position in the cycle. On the contrary in the case of filamentary discharges, the current signal in each half cycle is formed by several peaks which are not characterized by the same shape, amplitude and position in different cycles.[7-10]

The utilization of the above approach is not straightforward; as reported by Massines et al.,[10] for example, in the case of the glow DBD with helium and argon the amplitude of current peak is high and can encompass the current peaks due to microdischarges, as a consequence the analysis of the current signal does not allow an unambiguous definition of the discharge regime. On the contrary, for N_2 fed DBDs the current of the homogeneous Townsend-like discharge is low compared to that of the microdischarges and therefore the current measurement is sufficient to determine the presence of microdischarges. In fact, as soon as few MDs are formed, intense, narrow and well detectable current peaks clearly superimpose on the APTD signal. The contemporary use of the electrical diagnostics and an additional technique such as the high-speed imaging of the discharge (with exposure time comparable with MDs lifetime) allows to reduce this problem.[7-10, 19-21] For large area DBDs and for high current glow discharge, naked-eye observation of the discharge is particular useful because it allows to detect the formation of filaments (also if localized in small area regions of a prevalent homogeneous discharge) which

cannot be revealed with current measurements. Of course this does not exclude the existence of microdischarges and, therefore, that the discharge is not operating in a real homogeneous regime. The absence of visible filamentation is however a sufficient condition for a safe operation in surface processing of materials. For this reason, since in this work the evaluation of the discharge mode (diffuse or filamentary) is performed by naked-eye observations and electrical measurements, when the current signal is formed by only one peak per half-cycle and there is not any visible filamentation, we utilize the notation "*discharge of homogeneous appearance*" and not "*homogeneous discharge*". The electrical measurements and the naked eye observation performed under several experimental conditions showed that filamentation starts to be clearly visible when the relative standard deviation (RSD) of the amplitude of positive (or negative) current peaks is above 5% (calculated for five cycles).

Under the experimental conditions utilized in this study DBDs fed with He without additives are stable, distributed over the entire electrode surface and are of homogeneous appearance. DBDs fed with pure argon are distributed over the entire electrode surface and exhibit a homogeneous appearance at applied voltages below 5.4 kV_{p-p}, otherwise filaments can be clearly observed in some zones of the discharge gap. The addition of N_2, O_2, air and water vapor to helium or argon, under constant voltage and frequency conditions, can be responsible of two phenomena:

(i) The transition from a discharge of homogeneous appearance to a filamentary discharge if the additive concentration exceeds a threshold value "C_H". For instance, in the case of He-N_2 mixtures, at 20 kHz and 2.3 kV_{p-p} C_H occurs at 0.025% N_2. **Figure 2** shows that with a N_2 concentration lower than C_H (0.013%) the current exhibits the features of a homogeneous appearance discharge, while with 0.117% N_2 the current signal is typical of a filamentary discharge. A similar behavior is registered for DBDs fed with Ar, N_2 is characterized by a C_H of 0.35% at 20 kHz and 5.1 kV_{p-p}, a discharge of homogeneous

appearance is obtained at 0.125% of N_2 while filamentation is evident at 0.45% of N_2 (Figure 2).

(ii) The contraction of the discharge volume.[11] To obtain a quantitative evaluation of this phenomenon we define "C_{MAX}" as the concentration above which the discharge withdraws by more than 2 mm from one electrode edge. In the case of Ar-N_2 fed DBD, at 20 kHz and 4.8 kV_{p-p}, C_{MAX} is 0.3%. Therefore, as it can be appreciated in **Figure 3**, when the concentration of added N_2 is higher than this value the discharge is not distributed over the entire electrode surface. For a parallel-plate electrode DBD with lateral feed gas injection, like that utilized in this study, this phenomenon starts from the electrode edge close to the gas outlet. However it is worth to notice that at contaminant concentration higher than C_{MAX} a stable discharge occupying the entire interelectrodic volume can be restored by simply increasing the applied voltage. This indicates that feed additives increase the voltage necessary to sustain the discharge, as reported also by Brandenburg et al.[27] for air and nitrogen addition to helium or argon DBDs. The increase of the voltage necessary to sustain the discharge is likely a consequence of the discharge energy dissipation due, for instance, to the vibrational excitation of the molecular gas (N_2, O_2, H_2O) added to the noble gas. It is also reasonable that with increasing the distance from the gas inlet (i.e. with increasing the gas residence time into the discharge gap) this energy dissipation becomes more important and, as a consequence, the discharge quenching starts near to the gas outlet as shown in Figure 3.

As reported in **Figure 4**a, in He DBDs C_H values for N_2, O_2 and H_2O vapor do not depend on the applied voltage and the C_H for O_2 and H_2O (0.007% and 0.008%, respectively) are much lower than for N_2 (0.025%). In the case of air, C_H increases as a function of the applied voltage between

the values of N_2 and O_2. The higher C_H detected for N_2 can be related to the fact that N_2 is involved in indirect ionization processes (Penning ionization[8, 9, 27]) that favour the generation of a glow DBD. On the other hand O_2 and H_2O are electronegative gases (high oxygen electronegativity) that could destabilize the homogeneous regime for electron attachment.[30, 31] In agreement with this, it is worth to mention the results of Radu et al.[30, 31] who showed that in He DBDs the pseudoglow-to-filamentary transition occurs at higher added concentration for nitrogen respect to oxygen.

Figure 4b shows that in He fed DBD, C_{MAX} increases with the applied voltage for N_2, O_2, and air but not for H_2O which shows the lowest value (0.008 %). Also in this case, the behavior of air is intermediate between those of N_2 and O_2. The addition of the contaminants to He DBDs decreases the input power and the effect is more pronounced for O_2 and H_2O. At 1.7 kV_{p-p} the power decreases from 47 W to 35 W by adding 0.05% of O_2 or H_2O to helium.

In the case of Ar DBDs, the input power (36 W) is not affected by contaminants addition, C_H decreases as a function of the applied voltage and it is scaled as follows: $N_2 > air > H_2O \approx O_2$ (Figure 4c). The trends of C_{MAX} are similar to those observed for He (Figure 4d). The trend of C_{MAX} for water is not reported since the filamentary water contaminated discharges were characterized by intense and large radius filaments at the electrode edges at H_2O concentrations higher than 0.2%.

It is worth to highlight that while for helium the C_H is always lower than C_{MAX}, in some cases for argon the discharge contraction occurs before the transition from the homogeneous appearance to the filamentary regime.

Deposition of fluoropolymers in Ar-C_3F_6 DBDs

The deposition process of fluorocarbon thin films in Ar-C_3F_6 filamentary DBDs was first

investigated without contaminants addition, in order to define the overall performances: discharge regime, input power, deposition rate as well as chemical composition, wettability and morphology of the deposit. Under the selected experimental conditions (Table 1) a pure argon DBD is characterized by an eye detectable filamentary character, the current signal is formed by only one peak per half-cycle and the relative standard deviation of the current peaks amplitude is much higher than 5%. C_3F_6 addition results in an intense decrease of the discharge current and in the appearance of more current peaks per half-cycle, indicating a higher filamentary character of the discharge. At 0.2% of C_3F_6, the average power dissipated into the plasma decreases from 36 W (pure argon) to 22 W (Ar-0.2 % C_3F_6), the deposition rate is 56 $nm \cdot min^{-1}$ and the deposit is characterized by a high XPS F/C ratio of 1.7, as well as by AWCA and RWCA of 124° and 105°, respectively (film deposited in the middle of the interelectrode region). The main FT-IR spectral feature of the coating is the broad band between 900 and 1400 cm^{-1} (**Figure 5**a) due to the overlapping of some CF_x (x = 1-3) stretching vibration modes: [33, 36-39, 48, 49] i.e. the shoulder at 1350 cm^{-1} (CF), the peak at 1238 cm^{-1} with the shoulder at 1187 cm^{-1} (CF_2 asymmetric and symmetric stretching, respectively), and the peak at 980 cm^{-1} (CF_3). The weak and broad band between 1650 and 1850 cm^{-1} can be ascribed to the C=C stretching modes. The best fit of the XPS C1s signal (Figure 5b), performed with the five components reported in Table 2,[33, 36-40, 48, 49] shows that the CF_2 and CF_3 peaks are the most abundant (31% and 29%, respectively), indicating a low branching and cross-linking degree.[49] SEM observations show that the coating is smooth and powder free (**Figure 6**a).[49]

The UV-Vis emission spectra of the DBD were characterized by intense Ar emissions,[49, 53, 56] by the emission bands of CF_2 (A^1B_1-X^1A_1 system)[49, 54-56] and CF ($B^2\Delta$-$X^2\Pi$ system)[49, 54-56] and by two continua centred at approximately 290 and 620 nm, ascribed to CF_2^+[49, 55, 56] and CF_3,[49, 55, 56] respectively.

GC-MS analyses show that C_3F_6 depletion is 41% and that the by-products detected in the exhaust gas are different from those reported by Ozaki et al. in He-C_3F_6 glow DBDs,[46] i.e. CF_4, C_2F_4, C_2F_6, C_4F_8 and C_5F_{12}. In this work, in fact, only linear and cyclic fluorocarbons containing 6-8 carbon atoms have been identified.[52] Among these, the presence of linear, branched and cyclic hexanes (i.e. n-perfluorohexane, perfluoro-2-methylpentane, perfluoro-cyclohexane) suggests the occurrence of monomer dimerization reactions. On the other hand, the presence of CF_3 units in some by-products (e.g. perfluoro-methylcyclohexane and perfluoro-dimethylcyclohexanes) is in agreement with the quite high concentration of CF_3 groups detected in the coating by XPS. The fact that no high molecular weight by-products have been detected in the exhaust in appreciable quantity and the absence of powders, never detected by SEM, induce to consider the contribution of gas phase reactions to the polymerization process quite low; gas-surface heterogeneous reactions, involving low molecular weight fragments (e.g., with a molecular weight close to the C_3F_6 one), seem to play the major role in the deposition process.

The addition of contaminants reduces the power dissipated by the discharge (**Figure 7**a), the effect is higher for O_2 and H_2O. The C_{MAX} value detected for the various contaminants are reported in Table 3.

Figure 7 shows that, while the contaminant addition decreases the deposition rate, the chemical composition (and the wettability) of the coatings remains unchanged (constant XPS F/C ratio) and the oxygen and nitrogen uptake is always lower than 1% (film deposited in the middle of the interelectrode region). These results appear to be quite different from what reported in low pressure plasmas by Chen et al.,[37] in fact these authors observed N and O uptake as high as 9%.

A variation of film morphology due to the appearance of a slight roughness, more evident for the addition of air and oxygen than H_2O, can be appreciated (Figures 6b, c and d), while smooth coatings are obtained with N_2 addition (Figure 6e). Oxygen and air addition increases the

roughness of the deposits, likely due to contemporaneous etching reactions.

Figure 8 shows the deposition rate and the XPS F/C ratio of the coatings deposited in three different regions of the interelectrode zone i.e. at 1–6 cm, 8–13 cm and 15–20 cm from the gas entrance inside the discharge. The deposition rate exhibits a maximum as a function of the position in the discharge area (Figure 8a); the contaminants addition (0.1% Air and 0.05% H_2O) results in a decrease of the deposition rate at the positions 8–13 cm and 15–20 cm. The chemical composition of the coatings remains unchanged (constant XPS F/C ratio) over the entire electrode surface for both Ar-0.2% C_3F_6 and Ar-0.2% C_3F_6-0.1% Air mixtures, while a slight decrease of the F/C ratio is observed at the positions 1–6 cm and 8–13 cm in the case of Ar-0.2% C_3F_6-0.05% H_2O fed FDBDs.

Contaminants addition does not induce any important variation of the UV-Vis emissions observed without contaminants. When air is added to the feed gas, any signals from oxygen containing species is not detected, while intense emissions from the N_2 Second Positive System and the CN violet system band are observed.[54] With water addition, the OH emission ($A^2\Sigma^+$ - $X^2\Pi$ system) is detected.[54]

The depletion of C_3F_6 is 37% and 36% at the highest concentration of air (0.1%) and water vapor (0.05%), respectively, and is close to that measured without contaminants, indicating a quite similar monomer activation. The by-products observed with Ar-C_3F_6 fed DBDs are detected in similar amounts (flow rates in the range 0.1-0.01 sccm) also with air- and H_2O-containing feeds; only traces (below the quantification limit of 0.001 sccm) of new by-products, i.e. perfluoroacetone and trifluoroacetic acid, have been detected.

It seems that the presence of air and water vapor, and hence the occurrence of reactions involving these contaminants, does not change significantly the monomer activation, the nature of film precursors and hence the chemical composition of the deposit. However contaminants addition

seems to affect the discharge power and the deposition rate and, consequently, it is likely responsible of a decrease of the concentration of thin film precursors.

Conclusion

In this work the influence of N_2, O_2, air and water vapor feed gas impurities on the operation of DBDs fed with helium and argon was investigated. For each contaminant two different threshold concentration limits were assessed: C_H, namely the highest level of contaminant concentration above which the transition from a homogeneous to a filamentary regime can be observed; C_{MAX}, that is the contaminant concentration over which the discharge does not cover the entire electrode surface and begins to contract starting from the gas outlet side of the electrode system. With O_2 and H_2O the lowest C_H and C_{MAX} values were registered, while air generally exhibits an intermediate behavior between N_2 and O_2.

The effect of feed gas impurities on the PE-CVD of fluoropolymers in filamentary DBDs was also evaluated. Contaminants addition does not appreciably affect the chemical composition and the hydrophobic character of the deposited coatings, but it results in a decrease of the discharge power, of the deposition rate and in the appearance of a certain roughness; these changes are more evident for the addition of O_2, air and H_2O than for N_2. It has been supposed that oxygen is the main responsible for the power and deposition rate decrease observed with air addition, as well as for the appearance of the surface roughness that could be ascribed to the etching of the growing polymer.

The fact that the contaminants addition does not affect the chemical composition of the deposited film, the C_3F_6 depletion and the distribution of by-products allows to enhance the hypothesis that feed contaminants do not change the nature of the film precursors, but could be responsible of a decrease of the their concentration and hence of the deposition rate. Further studies will be

performed in order to confirm this hypothesis.

Acknowledgments: The authors gratefully acknowledge Mr. *Giovanni Di Renzo* for the scientific collaboration, Mr. *Savino Cosmai* for the technical assistance and Mrs. *Roberta Giordano* for the photographs of the discharge. This research has received financial support from *Regione Puglia* ("Accordo di programma quadro ricerca scientifica, II atto integrativo", project n. 51 "LIPP").

Keywords: dielectric barrier discharges (DBD), plasma-enhanced chemical vapor deposition (PECVD), fluoropolymers, gas impurities

References

[1] U. Kogelschatz, B. Eliasson, W. Egli , *J. Phys. IV France* **1997**, *7*, C4.

[2] U. Kogelschatz, *Plasma Chem. Plasma Process.* **2003**, *23*, 1.

[3] K. H. Becker, U. Kogelschatz, K. H. Schoenbach, R. J. Barker, *Non-Equilibrium Air Plasmas at Atmospheric Pressure*, Institute of Physics Publishing, Bristol 2005.

[4] A. Fridman, A. Chirokov, A. Gutsol, *J. Phys. D. Appl. Phys.* **2005**, *38*, R1.

[5] A. Fridman, *Plasma Chemistry*, Cambridge University Press, New York 2008.

[6] U. Kogelschatz, *IEEE Trans. Plasma Sci.* **2002**, *30*, 1400.

[7] F. Massines, G. Gouda, N. Gherardi, M. Duran, E. Croquesel, *Plasmas Polym.* **2001**, *6*, 35.

[8] F. Massines, P. Ségur, N. Gherardi, C. Khamphan, A. Ricard, *Surf. Coat. Technol.* **2003**, *174-175*, 8.

[9] F. Massines, N. Gherardi, N. Naudé, P Ségur, *Plasma Phys. Controll. Fusion* **2005**, *47*, B577.

[10] F. Massines, N. Gherardi, N. Naudé, P. Ségur, *Eur. Phys. J. Appl. Phys.* **2009**, *47*, 22805.

[11] F. Fanelli, *Surf. Coat. Technol.* **2010**, *205*, 1536.

[12] S. Kanazawa, M. Kogoma, T. Moriwaki, S. Okazaki, *J. Phys. D: Appl. Phys.* **1988**, *21*, 838.

[13] T. Yokoyama, M. Kogoma, T. Moriwaki, S. Okazaki, *J. Phys. D: Appl. Phys.* **1990**, *23*, 1125.

[14] L. Mangolini, K. Orlov, U. Kortshagen, J. Heberlein, U. Kogelschatz, *Appl. Phys. Lett.* **2002**, *80*, 1722.

[15] H. Luo, Z. Liang, B. Lv, X. Wang, Z. Guan, L. Wang, *Appl. Phys. Lett.* **2007**, *91*, 231504.

[16] Y. P. Raizer, *Gas Discharge Physics*, Springer, Berlin 1991.

[17] Y. B. Golubovskii, V. A. Maiorov, J. Behnke and J. F. Behnke, *J. Phys. D: Appl. Phys.* **2002**, *35*, 751.

[18] S. F. Miralaï, E. Monette, R. Bartnikas, G. Czeremuszkin, M. Latrèche, M. R. Wertheimer, *Plasmas Polym.* **2000**, *5*, 63.

[19] S. A. Starostin, M. A. M. ElSabbagh, E. Aldea, H. de Vries, M. Creatore, M.C.M. van de Sanden, *IEEE Trans. Plasma Sci.* **2008**, *36*, 968.

[20] S. A. Starostin, P. A. Premkumar, M. Creatore, E. M. van Veldhuizen, H. de Vries, R. M. J. Paffen, M. C. M. Van de Sanden, *Plasma Sources Sci. Technol*. **2009**, *18*, 045021.

[21] S. A. Starostin, P. A. Premkumar, M. Creatore, H. de Vries, R. M. J. Paffen, M. C. M. Van de Sanden, *Appl. Phys. Lett.* **2010**, *96*, 061502.

[22] US5414324 (1995) The University of Tennessee Research Corporation, invs.: J. R. Roth, P. Tsai, C. Liu, M. Laroussi, P. D. Spence.

[23] Z. Chen, *IEEE Trans. Plasma Sci.* **2002**, *30*, 1922.

[24] E. Aldea, P. Peeters, H. de Vries and M.C.M van de Sanden, *Surf. Coat. Technol.* **2005**, *200*, 46.

[25] US6774569 B2 (2004), Fuji Photo Film B.V., invs.: H. W. de Vries, F. Mori, E. Aldea, M. C. M. van de Sanden.

[26] EP 1626613 A1 (2006) Fuji Photo Film B.V., invs.: H. de Vries, J. Bouwstra, E. Aldea, M. C. M. van de Sanden, P. Peeters.

[27] R. Brandenburg, Z. Navrátil, J. Jánský, P. St'ahel, D. Trunec, H.-E. Wagner, *J. Phys. D: Appl. Phys.* **2009**, *42*, 085208.

[28] S. Okazaki, M. Kogoma, M. Uehara, Y. Kimura, *J. Phys. D: Appl. Phys.* **1993**, *26*, 889.

[29] J. R. Roth, J. Rahel, X. Dai, D. M. Sherman, *J. Phys. D: Appl. Phys.* **2005**, *38*, 555.

[30] I. Radu, R. Bartnikas, M. R. Wertheimer, *IEEE Trans. Plasma Sci.* **2003**, *31*, 1363.

[31] I. Radu, R. Bartnikas, M. R. Wertheimer, *J. Phys. D: Appl. Phys.* **2005**, *38*, 539.

[32] A. S. Chiper, R. Cazan, G. Popa, *IEEE Trans. Plasma Sci.* **2008**, *36*, 2824.

[33] F. Fanelli, R. d'Agostino, F. Fracassi, *Plasma Process. Polym.* **2007**, *4*, 797.

[34] EP 2024533 A1 (2009) Fuji Photo Film B.V., invs.: H. W. de Vries, E. Aldea, S. A. Starostin, M. Creatore, M. C. M. van de Sanden.

[35] P. A. Premkumar, S. A. Starostin, H. de Vries, R. M. J. Paffen, M. Creatore, T. J. Eijkemans, P.M. Koenraad, M. C. M. van de Sanden, *Plasma Process. Polym.* **2009**, *6*, 693.

[36] R. Chen, V. Gorelik, M. S. Silverstein, *J. Appl. Polym. Sci.* **1995**, *56*, 615.

[37] R. Chen, M. S. Silverstein, *J. Appl. Polym. Sci. A: Polym. Chem.* **1996**, *34*, 207.

[38] L. Sandrin, M. S. Silverstein, E. Sacher, *Polymer* **2001**, *42*, 3761.

[39] M. D. Garrison, R. Luginbühl, R. M. Overney, B. D. Ratner, *Thin Solid Films* **1999**, *352*, 13.

[40] E. Sardella, F. Intranuovo, P. Rossini, M. Nardulli, R. Gristina, R. d'Agostino, P. Favia, *Plasma Process. Polym.* **2009**, *6*, S57.

[41] T. Yokoyama, M. Kogoma, S. Kanazawa, T. Moriwaki, S. Okazaki, *J. Phys. D: Appl. Phys.* **1990**, *23*, 374.

[42] M. Kogoma, R. Prat, T. Suwa, A. Takeda, S. Okazaki, T. Inomata, in *Plasma Processing of Polymers*, R. d'Agostino, P. Favia, F. Fracassi eds., Kluwer Acad. Publ., NATO ASI Series, E: Appl. Sci., 346, Dordrecht 1997, p. 379.

[43] R. Prat, Y. J. Koh, Y. Babukutty, M. Kogoma, S. Okazaki, M. Kodama, *Polymer* **2000**, *41*, 7355.

[44] K. Tanaka, M. Kogoma, *Plasmas Polym.* **2003**, *8*, 199.

[45] Y. Yanagawa, Y. Masutani, M. Kogoma, K. Tanaka, *Thin Solid Films* **2007**, *515*, 4116.

[46] R. Ozaki, M. Kogoma, K. Tanaka, *Thin Solid Films* **2010,** *518*, 3566.

[47] R. Thyen, A. Weber, C.-P. Klages, *Surf. Coat. Technol.* **1997**, *97*, 426.

[48] F. Fanelli, F. Fracassi, R. d'Agostino, *Plasma Process. Polym.* **2007**, *4*, S430.

[49] F. Fanelli, G. Di Renzo, F. Fracassi, R. d'Agostino, *Plasma Process. Polym.* **2009**, *6*, S503.

[50] G. Beamson, D. Briggs, *High Resolution XPS of Organic Polymers*, J. Wiley & Sons, Chichester 1992.

[51] NIST and Wiley libraries in MassLab Release 1.4 (GC/MS Data System Software Finngan).

[52] F. Fanelli, S. Lovascio, R. d'Agostino, F. Fracassi, *Contr. Plasma Phys.*, DOI: 10.1002/ctpp.201000051.

[53] A. R. Striganov, N. S. Sventiskii, *Tables of Spectral Lines of Neutral and Ionized Atoms*, IFI/Plenum, New York and Washington 1968.

[54] R. W. B. Pearse, A. G. Gaydon, *The Identification of Molecular Spectra*, 4th edn., Chapman and Hall, London 1976.

[55] R. d'Agostino, F. Cramarossa, F. Fracassi, F. Illuzzi, in: *Plasma Deposition, Treatment and Etching of Polymers*, R. d'Agostino, Ed., Academic Press, New York 1990, p. 65.

[56] F. Fanelli, *Plasma Process. Polym.* **2009**, *6*, 547.

Figure captions

Figure 1. Schematic representation of the DBD reactor.

Figure 2. Current and voltage signals of He-N_2 fed DBDs (20 kHz, 2.3 $kV_{p\text{-}p}$) and Ar-N_2 fed DBDs (20 kHz, 5.1 $kV_{p\text{-}p}$): discharge of homogeneous appearance (He-0.013% N_2, Ar-0.125% N_2) and filamentary discharge (He-0.117% N_2, Ar-0.45% N_2).

Figure 3. Side-view of the Ar-N_2 fed DBDs at 20 kHz, 4.8 $kV_{p\text{-}p}$ and various N_2 concentrations (C_{MAX} = 0.3%).

Figure 4. Threshold concentrations, C_H and C_{MAX}, at 20 kHz as a function of the applied voltage for DBDs fed by He or Ar and additives (N_2, O_2, air, H_2O).

Figure 5. FT-IR spectrum (a) and XPS C1s signal (b) of film deposited in Ar-0.2% C_3F_6 fed FDBDs (15 kHz, 5.7 $kV_{p\text{-}p}$) in the middle of the interelectrode region.

Figure 6. SEM images of fluorocarbon films deposited in FDBDs fed with Ar-0.2% C_3F_6 (a) and with the addition of 0.1% air (b), 0.05% H_2O (c), 0.02% O_2 (d), 0.08% N_2 (e). Films are deposited in the middle of the interelectrode region.

Figure 7. Input power (a), deposition rate (b) and XPS F/C ratio (c) of fluoropolymers in Ar-0.2% C_3F_6 filamentary DBDs as a function of the contaminant concentration in the feed (15 kHz, 5.7 $kV_{p\text{-}p}$; contaminants: N_2, O_2, air, H_2O; film deposited in the middle of the interelectrode region).

Figure 8. Deposition rate (a) and XPS F/C ratio (b) of fluoropolymers deposited in FDBDs fed with Ar-0.2% C_3F_6, Ar-0.2% C_3F_6-0.1% Air and Ar-0.2% C_3F_6-0.05% H_2O, as a function of the position in the discharge area, i.e. at 1–6 cm, 8–13 cm and 15–20 cm from the gas entrance inside the discharge.

Table 1. Experimental parameters employed in this work.

	He	**Ar**	**Ar-0.2%C_3F_6**
Frequency, f (kHz)	20	20	15
Applied voltage, V_a (kV_{p-p})	1.5 – 2.5	2.6 – 5.7	5.7
Gas gap (mm)	5	2	2
Main gas flow rate (slm)	6	4	4
[N_2] (%)	0 – 0.6	0 – 1.5	0 – 0.4
[O_2] (%)	0 – 0.3	0 – 0.5	0 – 0.05
[Air] (%)	0 – 0.4	0 – 2.0	0 – 0.2
[H_2O] (%)	0 – 0.1	0 – 0.3	0 – 0.1

Table 2. Components used for the curve fit of XPS C1s of the fluorocarbon coatings.[33, 36-40, 48, 49]

	Binding energy **———————** **eV**	**C1s component**
1	285.0 + 0.2 eV	C-C
2	288.0 ± 0.3 eV	C-CF/CF=C
3	290.1 ± 0.3 eV	CF
4	292.5 ± 0.2 eV	CF_2
5	294.5 ± 0.2 eV	CF_3

Table 3. C_{MAX} values and $C_{MAX}/[C_3F_6]$ ratios for Ar-C_3F_6 DBDs.

	C_{MAX}	$C_{MAX}/[C_3F_6]$
	%	
N_2	0.2	1.0
O_2	0.025	0.125
Air	0.1	0.5
H_2O	0.05	0.25

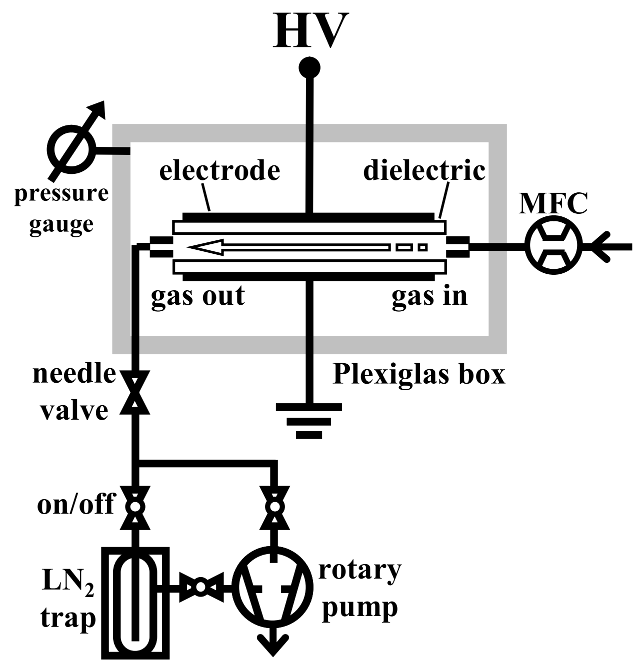

Figure 1. Schematic representation of the DBD reactor.

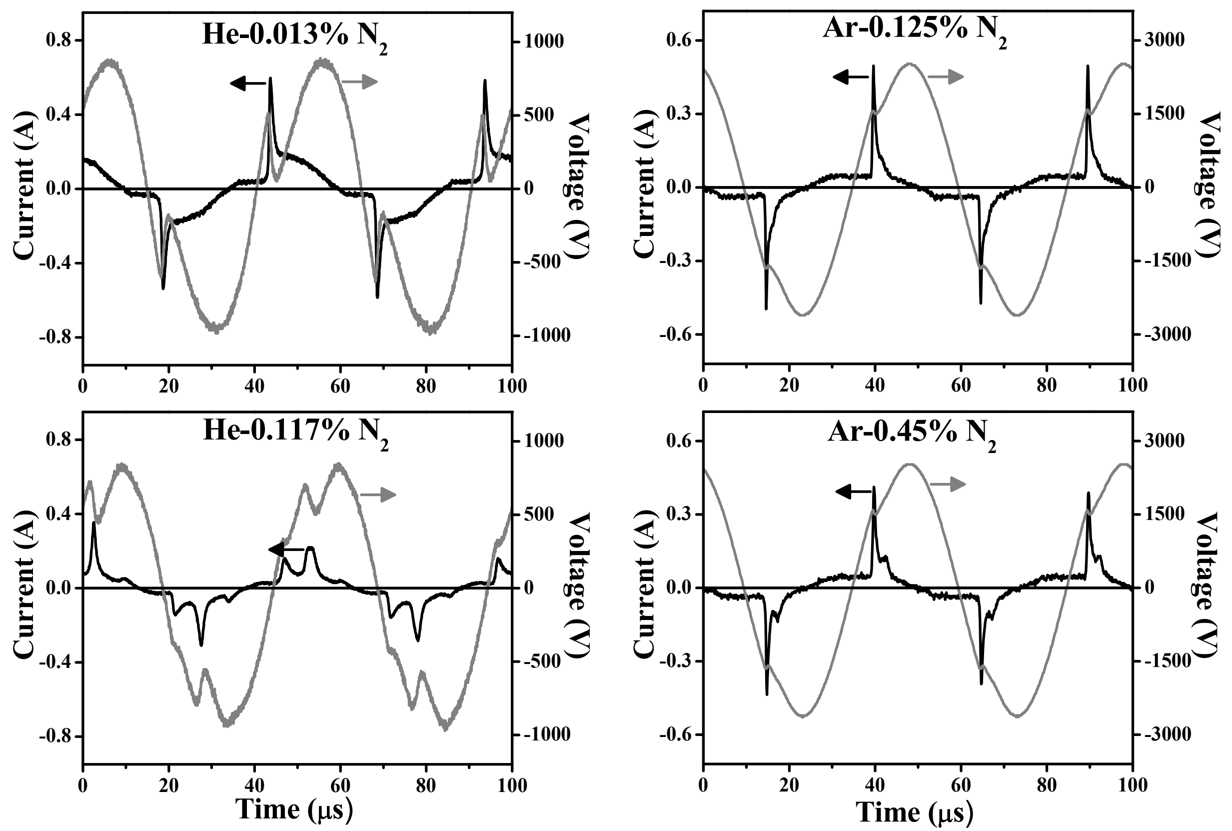

Figure 2. Current and voltage signals of He-N_2 fed DBDs (20 kHz, 2.3 $kV_{p\text{-}p}$) and Ar-N_2 fed DBDs (20 kHz, 5.1 $kV_{p\text{-}p}$): discharge of homogeneous appearance (He-0.013% N_2, Ar-0.125% N_2) and filamentary discharge (He-0.117% N_2, Ar-0.45% N_2).

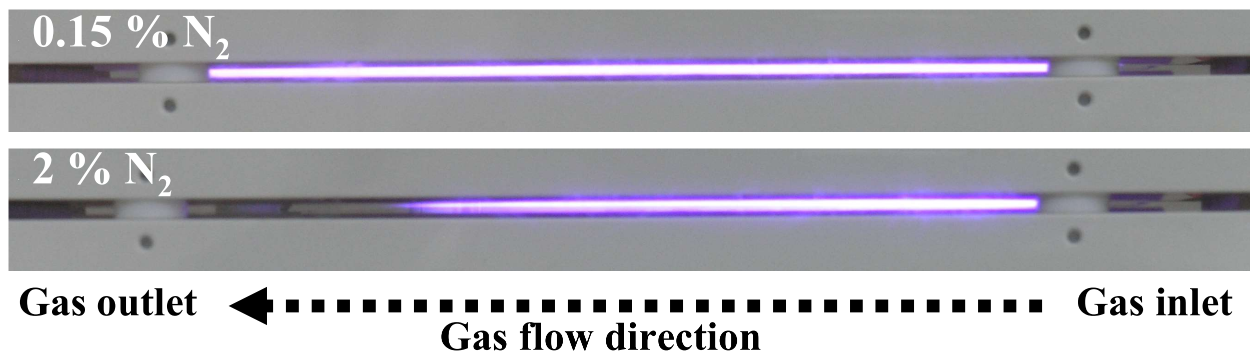

Figure 3. Side-view of the Ar-N_2 fed DBDs at 20 kHz, 4.8 kV_{p-p} and various N_2 concentrations (C_{MAX} = 0.3%).

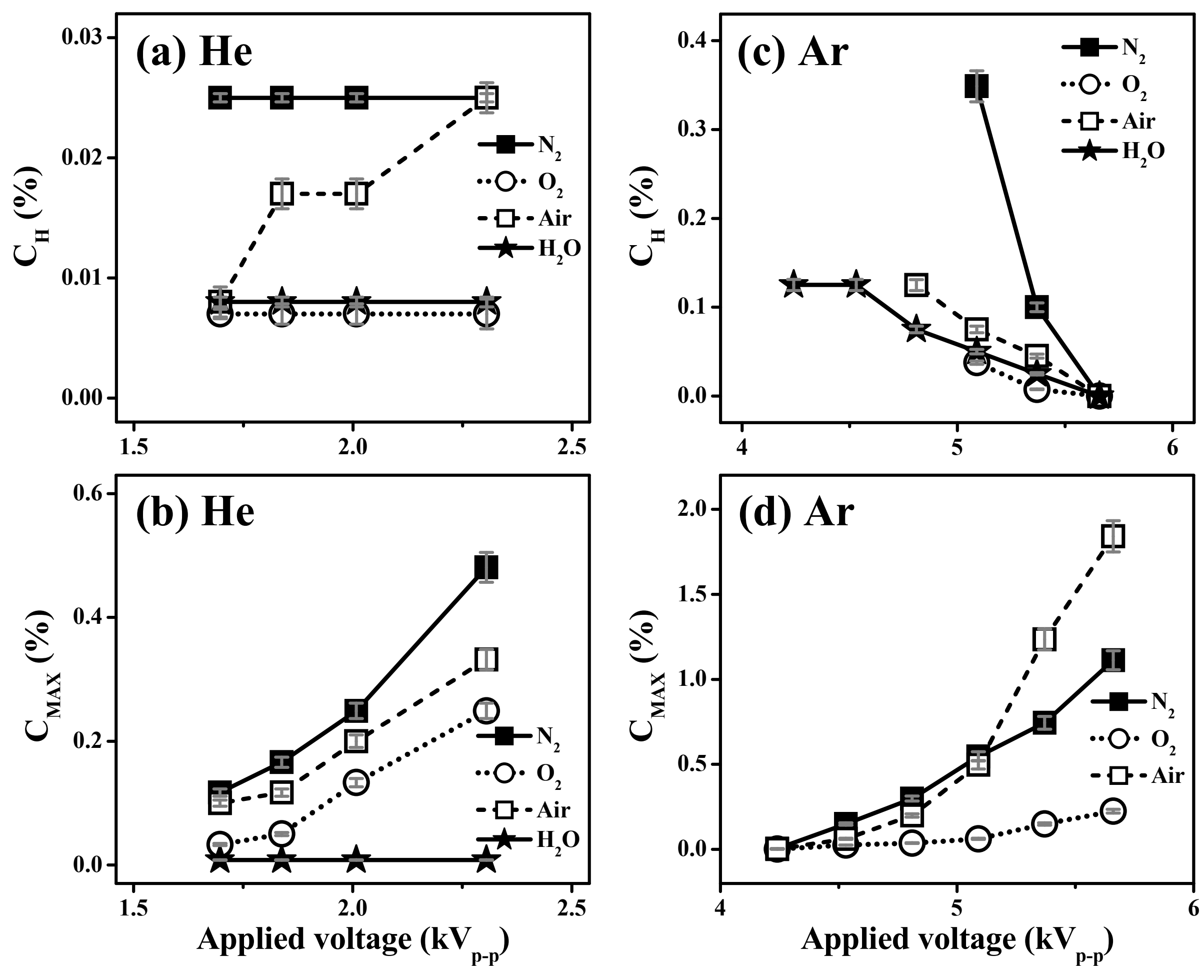

Figure 4. Threshold concentrations, C_H and C_{MAX}, at 20 kHz as a function of the applied voltage for DBDs fed by He or Ar and additives (N_2, O_2, air, H_2O).

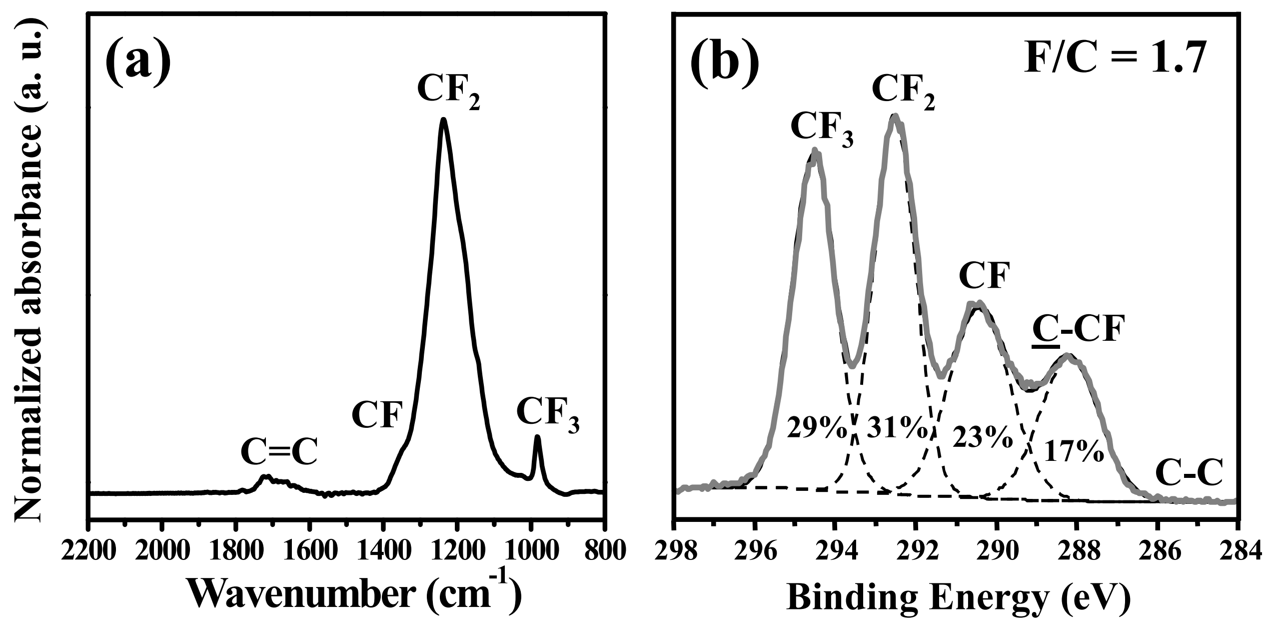

Figure 5. FT-IR spectrum (a) and XPS C1s signal (b) of film deposited in Ar-0.2% C_3F_6 fed FDBDs (15 kHz, 5.7 kV_{p-p}) in the middle of the interelectrode region.

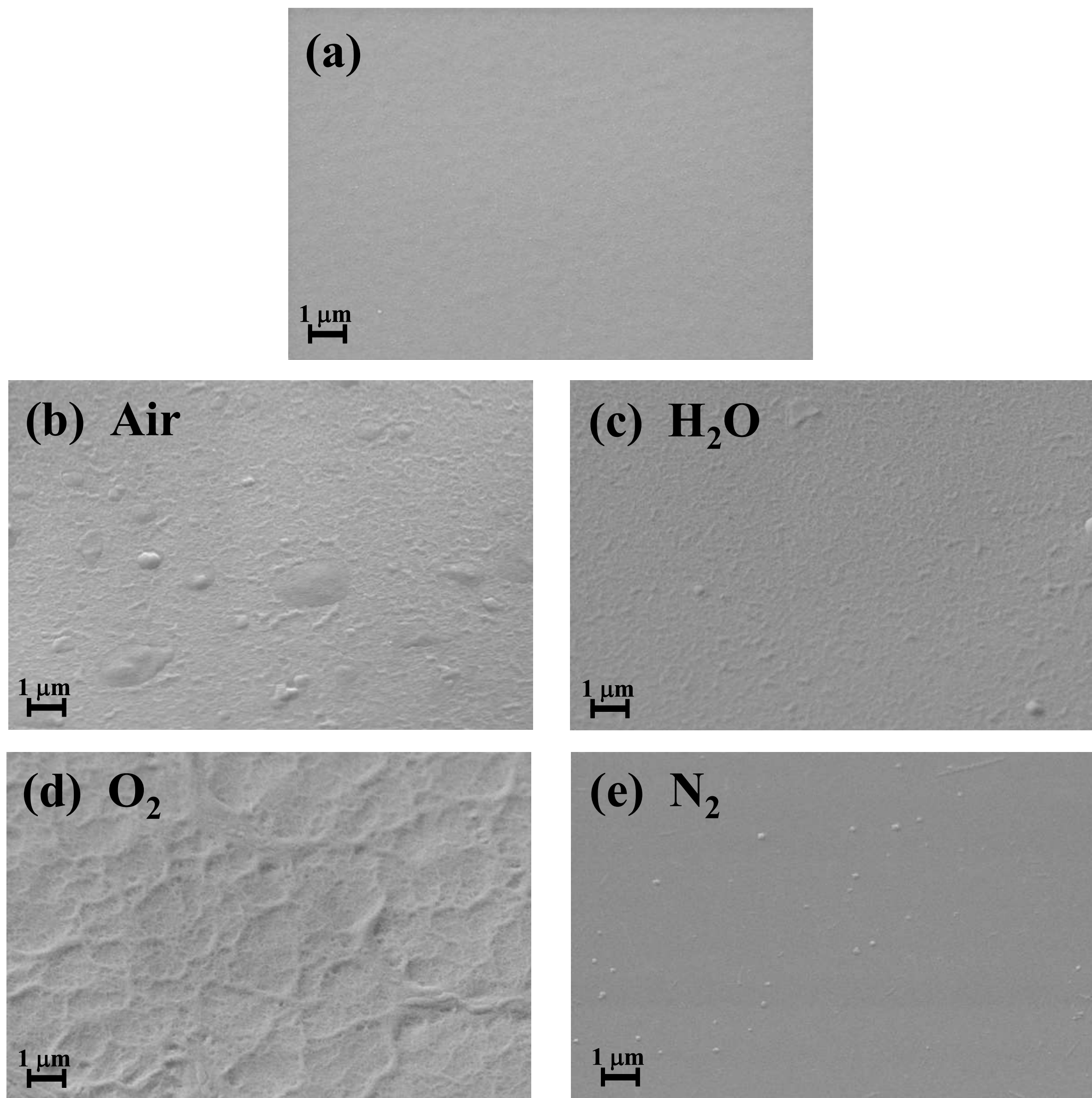

Figure 6. SEM images of fluorocarbon films deposited in FDBDs fed with Ar-0.2% C_3F_6 (a) and with the addition of 0.1% air (b), 0.05% H_2O (c), 0.02% O_2 (d), 0.08% N_2 (e). Films deposited in the middle of the interelectrode region.

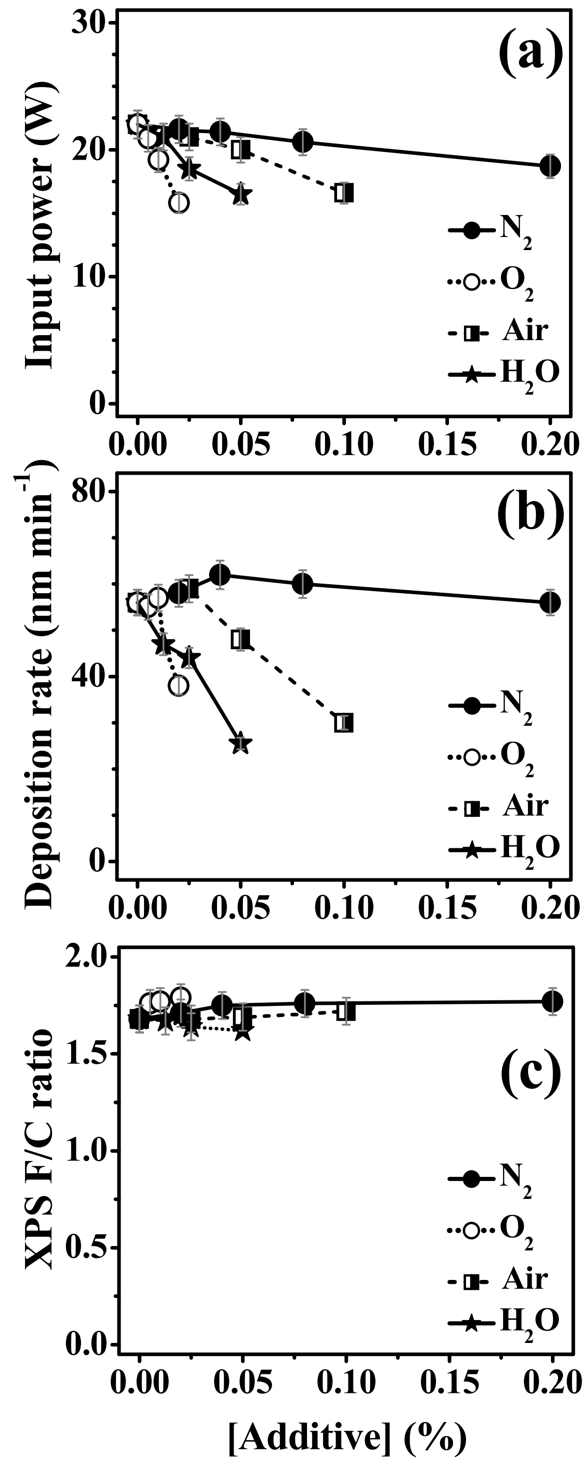

Figure 7. Input power (a), deposition rate (b) and XPS F/C ratio (c) of fluoropolymers in Ar-0.2% C_3F_6 filamentary DBDs as a function of the contaminant concentration in the feed (15 kHz, 5.7 kV_{p-p}; contaminants: N_2, O_2, air, H_2O; film deposited in the middle of the interelectrode region).

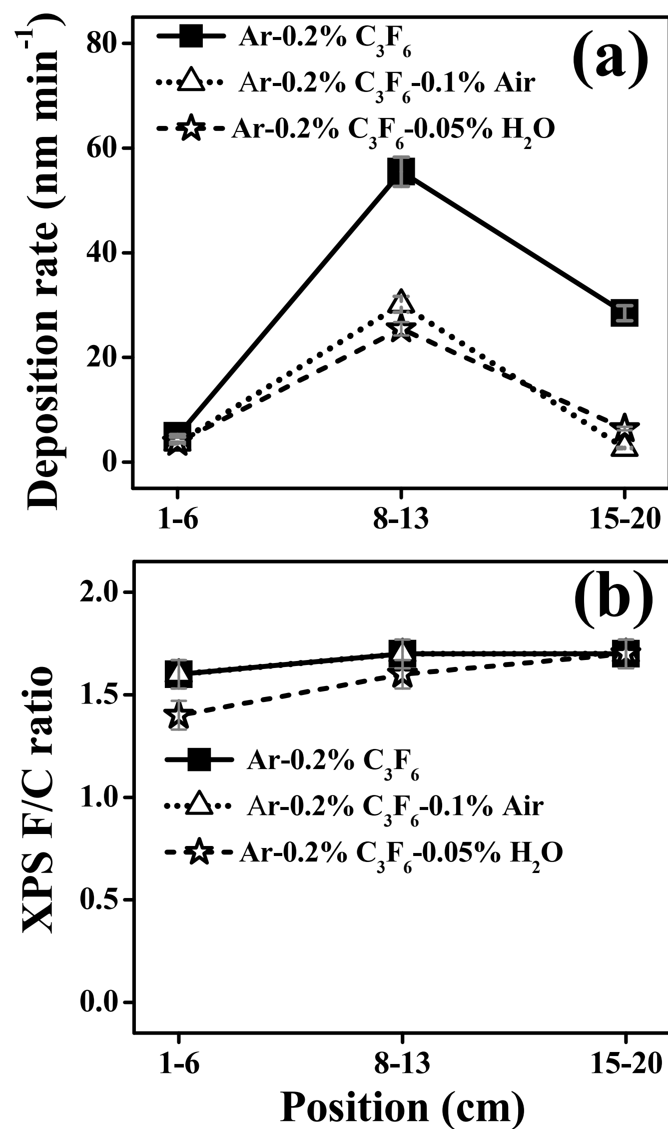

Figure 8. Deposition rate (a) and XPS F/C ratio (b) of fluoropolymers deposited in FDBDs fed with Ar-0.2% C_3F_6, Ar-0.2% C_3F_6-0.1% Air and Ar-0.2% C_3F_6-0.05% H_2O, as a function of the position in the discharge area, i.e. at 1–6 cm, 8–13 cm and 15–20 cm from the gas entrance inside the discharge.